

Facile Approach of Porous Electrochromic Polyamide/ZrO₂ Films for Enhancing Redox Switching Behavior

Ya-Wen Chiu, Min-Hao Pai, and Guey-Sheng Liou*

Cite This: *ACS Appl. Mater. Interfaces* 2020, 12, 35273–35281

Read Online

ACCESS |



Metrics & More



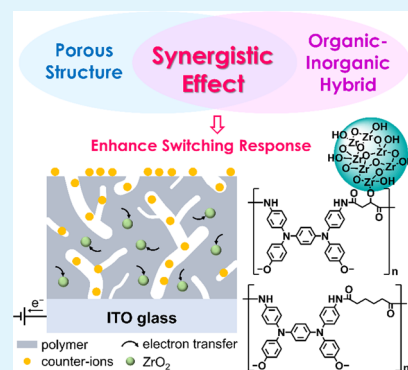
Article Recommendations



Supporting Information

ABSTRACT: Porous redox-active polyamide hybrid films have been successfully prepared to enhance the electrochromic (EC) properties in this report comparing with salt-caused porous films and hybrid films obtained via *in situ* sol–gel reaction of hydroxyl groups and zirconium dioxide (ZrO₂). With the assistance of porous and hybrid structures, the diffusion rate of counterions between electrolyte and EC species could be effectively increased, and the charges could be delivered and stored between the donor–acceptor system constructed by the organic–inorganic hybrid during the electrochemical process. Furthermore, there would be a synergistic effect while combining the porous structure and hybrid system together, which can improve the EC behaviors much more obviously; that is, the enhancement of porous hybrid films is more than that of porous films and hybrid films individually. For further application, the porous hybrid films were fabricated into devices, which exhibit a lower oxidation potential (from 1.07 to 0.94 V) and shorter switching response time (from 81.3 to 9.7 s for coloring time and from 44.7 to 20.8 s for bleaching time) with good electrochemical stability. Consequently, these results indicate that the EC properties could be enhanced and improved dramatically by the facile approach of merging the porous structure and hybrid system.

KEYWORDS: electrochromic polyamide film, salt-caused porous structure, sol–gel, ZrO₂ hybrid, electrochromic switching response



1. INTRODUCTION

In the recent information age, the technology of display is one of the critical techniques. The diverse demands from mature consumers have triggered scientists to pursue new technologies and sprang up diversified products to meet the needs. The materials with the features of high flexibility, high transparency, and energy-saving are the focus of the latest research trend. One of the most attractive optical materials should be applied for the fabrication of electrochromic devices (ECDs), which could show the phenomenon of reversible color changing caused by different optical absorptions during electrochemical redox procedures. Due to their obvious optical contrast ratio, high coloration efficiency, fast switching response capability, and good stability, electrochromic (EC) materials have been believed to be promising candidates for the application of display and optoelectronic materials; therefore, various EC materials have been developed and investigated since the 1960s.^{1,2} To date, EC materials can be divided into several major categories, such as transition metal oxides (e.g., tungsten trioxide (WO₃)³ and nickel oxide (NiO)^{4–6}), coordination complexes (e.g., Prussian blue (PB)^{7,8}), small organic molecules (e.g., viologen^{9,10}), conjugated polymers (e.g., polyaniline (PANI)^{11,12}), and metallopolymer (e.g., ruthenium polypyridyl and metallo-supramolecular polymers^{13,14}). Among them, EC materials that consist of a polymer are in the

spotlight due to advantages of flexibility, low cost, good processing properties, and high optical performance.

Since 2005, our research group has focused on developing the triphenylamine-derived (TPA-derived) EC polyamides and polyimides.^{15,16} According to our recent research, EC polymers with high optical transparency and colorless appearance at the neutral state could be obtained while inducing various TPA moieties into the polymer backbone as electroactive groups. Furthermore, these EC materials possess a high optical contrast ratio during the redox process, which raises the potential for application of novel technology of display, especially the truly black display in the coloring state,^{17,18} attracting much attention from the industry.

However, from the applied perspective, the thickness of polymer films plays a crucial role in EC behaviors and optical properties. Normally, thicker films show a higher optical contrast ratio, which exhibits higher potential for application; nevertheless, they also have some negative impacts on other

Received: May 21, 2020

Accepted: July 15, 2020

Published: July 15, 2020



EC properties, such as higher oxidation potential, longer response time, and worse stability.

The reason is that as the thickness of films increases, the diffusion rate of counterions through the films becomes a more dominant step to demonstrate the most influence on the switching response time. Therefore, there are several methods having been proposed to improve the response time during the electrochromic process, such as incorporation of nanostructures^{19–23} and introduction of a charge-acceptor metal oxide^{24–27} as charge storage into EC materials. In this study, to improve these problems, two reported methods have been investigated: one is the introduction of a porous structure into polymer films by using electrolyte salts,²⁸ and the other is bringing in organic–inorganic polymer hybrids with titanium oxide (TiO₂).²⁹ These two methods not only show lower redox driving potentials and quick switching capability but also exhibit higher electrochemical stability.

Generally, by introducing a porous structure into polymer films, the surface area and channels throughout the whole polymer film should be increased to generate a shorter distance for charge transportation and facilitate the mobility of counterions while diffusing through the film; that is, the EC properties could be enhanced effectively via a porous structure. Recently, we have proposed a facile and useful method to produce porous polymer films by adding electrolyte salts into the polymer solution and then washing the salts out after casting the films onto the indium tin oxide (ITO) glass.^{30–32} Organic–inorganic hybrids are connected with covalent bonds via *in situ* sol–gel reaction by introducing carboxylic groups (–COOH) or hydroxyl groups (–OH) into the polymer chains to provide active sites to metal oxides (e.g., TiO₂ and ZrO₂). Through this approach, the metal oxides could distribute throughout the film evenly with a diameter of no more than 40 nm to avoid the optical transparency loss.^{33,34} Furthermore, the metal oxides could serve as the electron storage units to facilitate the charge transfer during the redox process, implying that metal oxides would store the electrons from the TPA-derived moieties during the electrochemical process, while they could transfer the electrons back to the centers in the reduction process. With the assistance of covalent bonds, the transfer would be facilitated to be even more effective and faster, which can be observed by the switching response time of the EC materials.

Herein, we propose a concept of combining a porous structure with an organic–inorganic hybrid into one system and successfully obtained the porous polyamide hybrid films, which possess a synergistic effect that could enhance EC behaviors, including switching response and stability, to perform them more effectively and obviously than either the porous polymer films or polymer hybrids (Figure 1).

2. RESULTS AND DISCUSSION

2.1. Optical Properties of Polyamide Films.

TPPA-A was used as the material for ECDs, which could exhibit different colors from transparent to black, and TPPA-M with hydroxyl groups was used for preparing hybrid films through *in situ* sol–gel reaction. The synthesis routes of TPPA-A and TPPA-M and the *in situ* sol–gel reaction of TPPA-M are illustrated in Scheme 1, and their inherent viscosities and molecular weights are listed in Table S1. The preparation routes of porous films, hybrid films, and porous hybrid films are illustrated in Figure S1. The porous films of TPPA-A and TPPA-M with different concentrations of electrolyte salt,

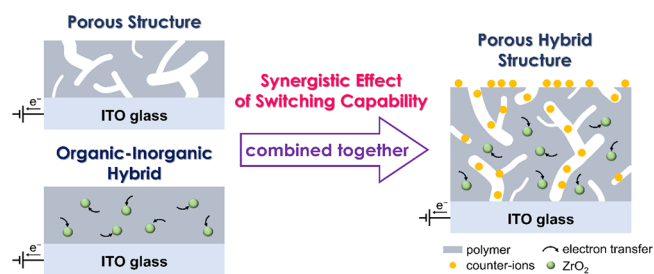


Figure 1. Illustration of the combination of the porous structure and organic–inorganic hybrid as a porous hybrid structure.

tetrabutylammonium tetrafluoroborate (TBABF₄), for generating the pores throughout the whole polymer films were prepared and named as A-Sx and M-Sx, where x is the concentration of TBABF₄. The UV–vis spectra of these porous films are shown in Figure S2. From the results, TPPA-A could maintain a high optical transparency up to 40 wt % concentration of TBABF₄ (Figure S2a), while the transparency of the TPPA-M porous film (Figure S2b) decreased obviously at the same salt concentration compared with TPPA-A, indicating that the amount of TPPA-M could impact the transparency of the porous films significantly. Therefore, only 35 wt % TPPA-M was added to TPPA-A to prepare polymer blend films for the following experiments.

The porous and hybrid films of polymer blend were named as Sa-Zrb, where a is the weight concentration of the salt for producing pores, and b is the weight percentage of ZrO₂ incorporated to the polymer by the sol–gel reaction. To maintain the same amount of EC materials for different modified systems, tuning the thickness of the corresponding films should be necessary, and the values are summarized in Table S2. The optical transmittance of the porous films before and after washing out the salt by acetonitrile shown in Figure 2 reveals no obvious transmittance loss up to 30 wt % TBABF₄ (S30-Zr0), while 40 wt % of the electrolyte system (S40-Zr0) caused a lower but acceptable transmittance compared to the pristine polymer blend film (S0-Zr0). However, the transmittance would decrease drastically when the weight percentage of TBABF₄ reached 50 wt % (S50-Zr0) even before the salts were washed out. Due to the low transparency, S50-Zr0 would not be applied in the following analysis. In addition, there was no obvious transmittance loss after the salts were washed out because it could be compensated by the electrolyte solution during the measurement of EC behaviors¹⁸ (Figure 2b). Furthermore, scanning electron microscopy (SEM) images reveal the smooth surface of S0-Zr0 and porous structure for S30-Zr0 containing the pores with a diameter around 2.0–3.0 μm dispersed throughout the whole polymer films (Figure 3). Additionally, the SEM cross-sectional image of the porous film indicates that the pores not only could form on the surface of films but also exist within the films (Figure 3b). Additionally, a smaller and deeper hole inside the shallow could be observed from the magnified overview of the holes (Figure 3d), revealing the connection of different pores throughout the film and the feasibility of producing porous channels by this method. From the aspect of transparency, 30 wt % TBABF₄ was the best concentration to prepare the porous film; therefore, this amount of TBABF₄ was added to prepare the targeted porous hybrid films with different ratios of ZrO₂. The transmittance of the hybrid films and porous hybrid films is shown in Figure 4. From the results,

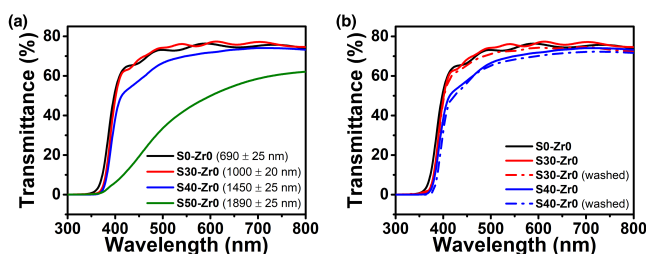
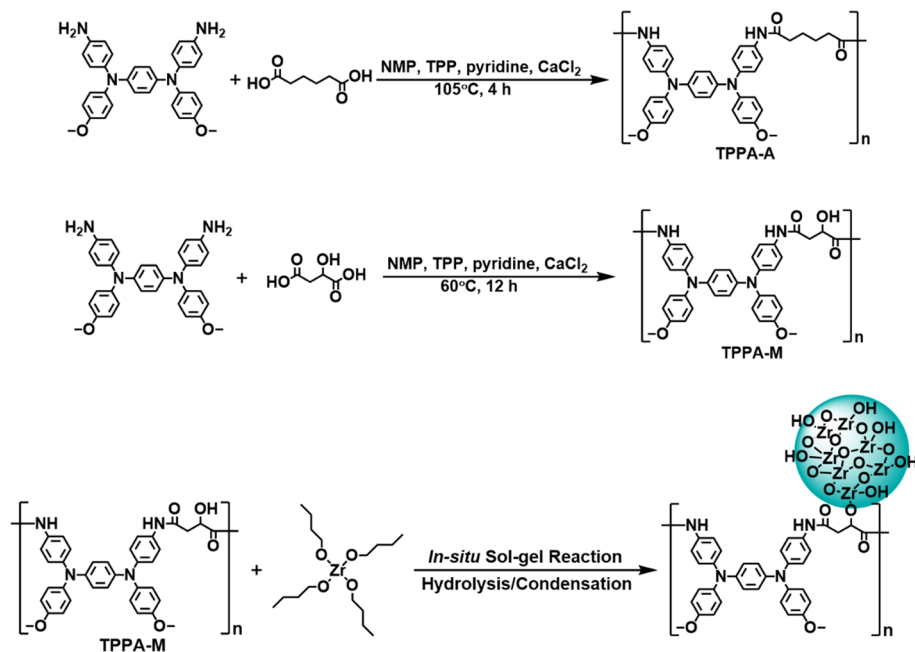
Scheme 1. Synthesis Routes of TPPA-A and TPPA-M and *In Situ* Sol–Gel Reaction of TPPA-M

Figure 2. UV–vis spectra of the porous films of polymer blends coated on ITO glasses (a) before and (b) after TBABF_4 was washed out (air as background). The spectrum of **S0-Zr0** is also added for comparison.

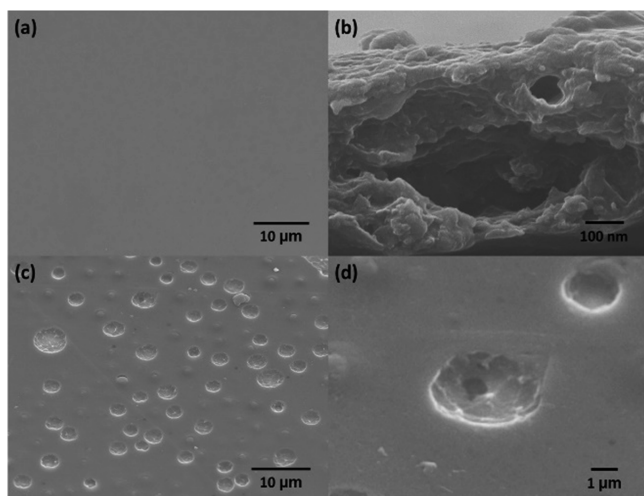


Figure 3. SEM images of (a) **S0-Zr0**, (b) cross section, (c) overview, and (d) magnification overview of **S30-Zr0**.

although the transparency decreased with increasing ratio of hybrid content, the addition of ZrO_2 up to 20 wt % did not cause so much transmittance loss as porous films.

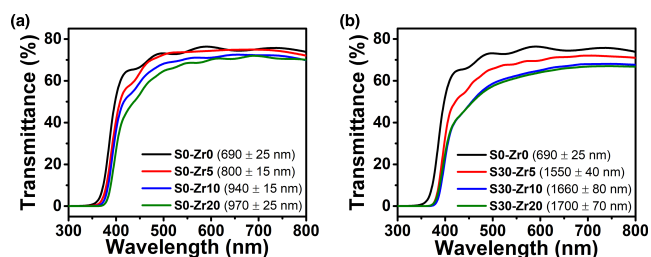


Figure 4. UV–vis spectra of (a) hybrid films and (b) porous hybrid films coated on ITO glasses (air as background). The spectrum of **S0-Zr0** is also added for comparison.

2.2. Electrochromic Properties of Polyamide Films.

2.2.1. Spectroelectrochemistry. The spectroelectrochemical spectra of **S0-Zr0** used for evaluating the optical behaviors of the EC polymer films are shown in Figure S3. The film of **S0-Zr0** showed a transparent pale yellow color at the neutral state (0 V), the intensity of characteristic peaks at 425, 600, and 920 nm increased, and the film displayed a green color with increasing applied potential. These characteristic peaks attained their maximum absorbance at around 0.45 V, which is the end of its first oxidation state.

Then, the absorbance at 425 nm decreased and the peaks at 600 and 920 nm slowly shifted to 620 and 780 nm, respectively, with a color change to blue at 0.8 V related to the second oxidation state of the film.

2.2.2. Electrochemical Properties. The electrochemical behavior of the films was investigated through cyclic voltammetry (CV) and the typical diagram for TPPA-derived polymers exhibited two reversible oxidation redox stages at around 0.4 and 0.8 V, respectively. Because of the lower oxidation potential and higher stability at the first oxidation stage, which could be more effective and useful for application, only the first oxidation redox behaviors will be discussed in this study. The CV diagrams of **S0-Zr0**, **S30-Zr0**, **S0-Zr20**, and **S30-Zr20** films are illustrated in Figure 5, and the related oxidation redox potentials are summarized in Table 1. Thus,

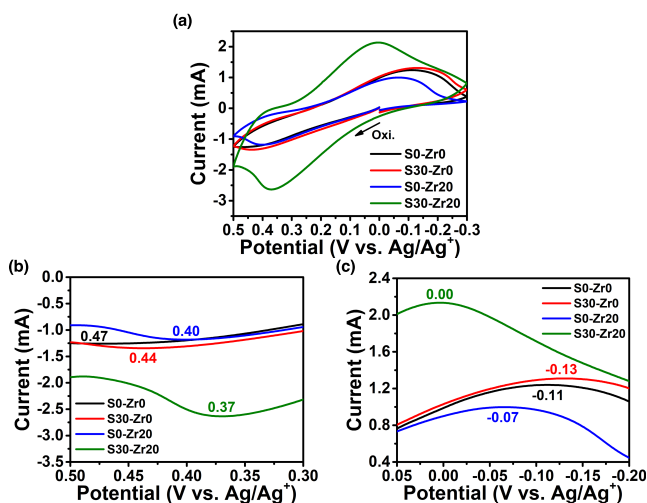


Figure 5. (a) CV diagrams of S0-Zr0 (thickness: 690 ± 25 nm), S30-Zr0 (thickness: 1000 ± 20 nm), S0-Zr20 (thickness: 970 ± 25 nm), and S30-Zr20 (thickness: 1700 ± 70 nm) films on the ITO-coated glass substrate (coated area: $0.6 \text{ cm} \times 3 \text{ cm}$) in $0.1 \text{ M TBABF}_4/\text{MeCN}$ at a scan rate of 50 mV/s , and the magnification of their (b) oxidation peaks and (c) reduction peaks.

Table 1. Redox Peak Potentials^a, Response Time, and Charge Transfer Resistance (R_{ct}) of S0-Zr0, S0-Zr20, S30-Zr0, and S30-Zr20

film	$E_{\text{oxi.}}^b$ [V]	$E_{\text{red.}}^c$ [V]	ΔE^d [V]	t_c^e [s]	t_b^f [s]	$R_{ct,0.45}^g$ [Ω]	$R_{ct,0}^h$ [Ω]
S0-Zr0	0.47	-0.11	0.58	12.9	83.4	61.5	71.9
S30-Zr0	0.44	-0.13	0.57	10.0	71.4	54.6	67.5
S0-Zr20	0.40	-0.07	0.47	8.4	41.7	39.0	48.7
S30-Zr20	0.37	0.00	0.37	6.4	14.9	32.6	36.4

^aMeasured relative to Ag/Ag⁺ in MeCN. ^bOxidation potential at the peak. ^cReduction potential at the peak. ^dPotential difference between oxidation and reduction peaks, $|E_{\text{oxi.}} - E_{\text{red.}}|$. ^eColoring time needed from the bleaching state to 90% of total transmittance change. ^fBleaching time needed from the coloring state to 90% of total transmittance change. ^gCharge transfer resistance obtained from the diameter of the semicircle or the arc at a coloring voltage of 0.45 V . ^hCharge transfer resistance at a bleaching voltage of 0 V .

introducing either the porous structure (S30-Zr0) or organic–inorganic hybrid (S0-Zr20) could lower the oxidation potentials. With the help of the porous structure, the supporting electrolyte could diffuse within the EC film more easily and effectively, and ZrO₂ could serve as electron storage units to accept electrons from the redox-active TPA-derived moieties via covalent bonds during the oxidation process. Not only were the oxidation potentials of S30-Zr0 (0.44 V) and S0-Zr20 (0.40 V) lower than that of S0-Zr0 (0.47 V), but S0-Zr20 also showed more obvious influence than S30-Zr0, indicating that the enhancement via the hybrid system is more effective than the porous structure. Compared to transferring through counterions, which need a longer period to diffuse between the electrolyte and electroactive species, the hybrid system behaved faster for transferring electrons from the redox-active TPA units to ZrO₂ connected to the polymer backbone via covalent bonds. Moreover, the electrons stored in the electron acceptor of ZrO₂ could also transfer back to the oxidized TPA moieties with a faster response rate during the reduction process, resulting in a lower reduction potential (-0.07 V) than S0-Zr0 (-0.11 V) and S30-Zr0 (-0.13 V).

When these two approaches were combined as one system, a synergistic effect could be generated, and both the resulting oxidation (0.37 V) and reduction (0.00 V) potentials could be further reduced than the corresponding values of S30-Zr0 and S0-Zr20, respectively. Additionally, the potential difference (ΔE) between the oxidation peak and reduction peak could be used to indicate the rate of electron transfer³⁵ and the driving capability of redox process. According to the results, both the ΔE values of S0-Zr20 (0.47 V) and S30-Zr0 (0.57 V) were lower than that of S0-Zr0 (0.58 V), and S0-Zr20 exhibited an even lower value than S30-Zr0.

Generally, larger ΔE means a lower transfer rate of electrons and larger force is necessary to drive the redox process; conversely, smaller ΔE represents the higher transfer rate of electrons that is beneficial to perform EC behaviors in a shorter response time. Therefore, S30-Zr20 (0.37 V) revealed the lowest ΔE , indicating the useful and effective synergistic effect of the porous structure and organic–inorganic hybrid. The CV diagrams of all the prepared films are depicted in Figure S4, and the values of related potentials are also summarized in Table S3.

2.2.3. Electrochromic Switching Properties. EC switching response behaviors were investigated at different driving potentials for these prepared films, and the absorption of the characteristic peaks was monitored as a function of time during the redox process. The values of switching time for the films of S0-Zr0, S30-Zr0, S0-Zr20, and S30-Zr20 are shown in Figure 6 and summarized in Table 1. For the measurement, the given

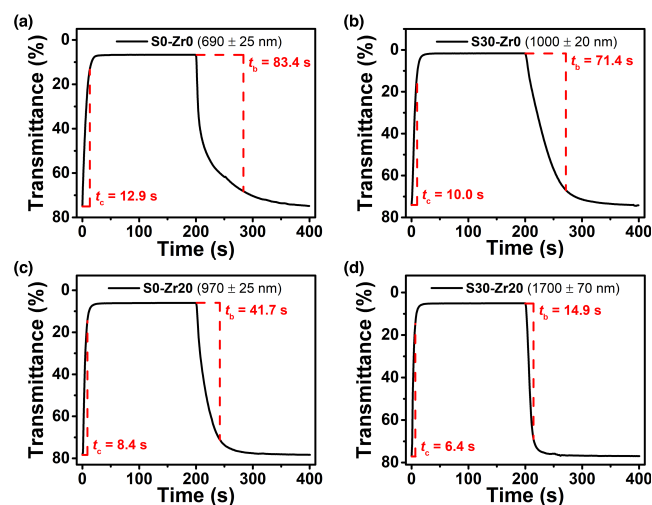


Figure 6. Switching response time of (a) S0-Zr0 (thickness: 690 ± 25 nm), (b) S30-Zr0 (thickness: 1000 ± 20 nm), (c) S0-Zr20 (thickness: 970 ± 25 nm), and (d) S30-Zr20 (thickness: 1700 ± 25 nm) films on ITO glasses (coated area: $0.6 \times 3 \text{ cm}$) at 920 nm in $0.1 \text{ M TBABF}_4/\text{MeCN}$ with 0.45 V as coloring voltage and -0.15 V as bleaching voltage.

wavelength was 920 nm , which referred to the spectroelectrochemical spectra in Figure S3, and the applied potentials were 0.45 and -0.15 V for coloring and bleaching, respectively, which were suitable potentials to complete oxidation and reduction for the EC films. The switching time was calculated at 90% of the full switch; coloring is the difference of transmittance from a neutral state to oxidation state, while bleaching is the change of transmittance from the oxidized form back to the original neutral state. From the results, the pure film S0-Zr0 revealed switching times of 12.9 s for coloring

and 83.4 s for bleaching; the porous film S30-Zr0 showed response times of 10.0 and 71.4 s for the coloring time and bleaching time, respectively (Figure 6b). In addition, the hybrid film S0-Zr20 exhibited response times of 8.4 s for coloring time and 41.7 s for bleaching time. Hence, both the porous film S30-Zr0 and hybrid film S0-Zr20 demonstrated a shorter response time. Compared to S30-Zr0, S0-Zr20 displayed much more impact on the response time, especially on the bleaching time; namely, films with a porous structure could allow counterions to diffuse between the electrolyte and electroactive species faster than pure films due to the channels provided, while the hybrid films could supply electron storage sites near the oxidation centers to shorten the response time more effectively than porous films because of the diffusing time saved. These two kinds of films mentioned above used different ways to advance the switching capability; therefrom, we can speculate that the porous hybrid films, a combination of those two approaches, should have even a shorter response time. This deduction was proved by the result of S30-Zr20 (Figure 6d); the coloring and bleaching times of S30-Zr20 could be shortened to 6.4 and 14.9 s, respectively, which are about half of the original values. The results suggested that when the two modifications were combined, the enhancement would be much more obvious. The values of other prepared films are also shown in Figures S5 and S6 and listed in Table S4.

2.2.4. Electrochemical Impedance Spectroscopy. Electrochemical impedance spectroscopy (EIS) is a common measurement to analyze the resistance of the electrode caused by interfacial charge transfer and mass transfer. Thus, it could be used in this study to provide a more convincing evidence toward the effect of both the porous structure and organic–inorganic hybrids.³⁶ The Nyquist plots of the resulting films are illustrated in Figure 7. Herein, these Nyquist plots were

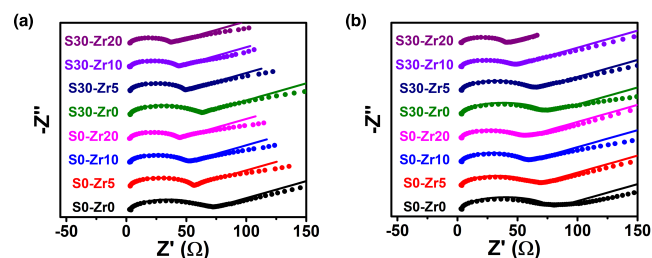


Figure 7. Nyquist plots of all the films at (a) 0.45 V and (b) 0 V.

fitted by an equivalent electrical circuit, Randles circuit, which consists of an active electrolyte resistance (R_{Ω}) in series with a parallel combination of a double-layer capacitance (C_d), an impedance of charge transfer resistance (R_{ct}), and Warburg element (Z_w). Based on the similar environment of the measuring system, R_{Ω} should be nearly the same, and R_{ct} would change with the characteristic of a different electrode; that is, the effect resulted from the porous structure and hybrid could be estimated by R_{ct} . The values of R_{Ω} and R_{ct} were obtained by applying potentials of 0.45 and 0 V to the films for investigating the electrochemical behaviors in both the coloring state and bleaching state, respectively (Table S5). No matter which potential was applied, the tendencies are similar. Consequently, S0-Zr0 exhibited the largest R_{ct} (61.5 Ω at 0.45 V and 71.9 Ω at 0 V), implying a slower electron transfer rate. If the R_{ct} would be lowered by introducing a

porous structure or the hybrid content into the polymer films, then these two architectures could enhance the capability of charge transfer to facilitate a faster switching response in EC materials. Furthermore, EC films with the combination of porous and hybrid structures exhibited lower values of R_{ct} than their corresponding pristine polymer films, porous films, and hybrid films, respectively. The representative porous hybrid film S30-Zr20 demonstrated the lowest R_{ct} (32.6 Ω at 0.45 V and 36.4 Ω at 0 V). At the same time, the values of R_{Ω} and R_{ct} at 0.45 V were both smaller than those at 0 V, corresponding to the relation of coloring time and bleaching time (Tables S4 and S5), implying that these EC films possessed a higher rate of charge transfer in the oxidation than the reverse reduction processes. Consequently, the higher charge transfer rate caused by the more efficient diffusion of the electrolyte counterions and electron storage effect from the electron acceptor of ZrO₂ could effectively promote the response capability of EC films for both coloring and bleaching procedures.

2.3. Electrochromic Properties of ECDs. For further application, some representative EC films, S0-Zr0, S30-Zr0, S0-Zr20, and S30-Zr20, mentioned above were chosen for comparison to fabricate ECDs with a gel-type electrolyte and to check if the porous structure and hybrid system still reveal a duplicated effect in ECDs when they were merged.

2.3.1. Electrochemical Properties. With the help of HV, the ambipolar EC devices could be constructed with TPA-derived polymer films, the applied potentials of the first and second oxidation states for S0-Zr0/HV were 1.07 and 1.46 V, respectively (Figure 8a). HV²⁺ could accept electrons from

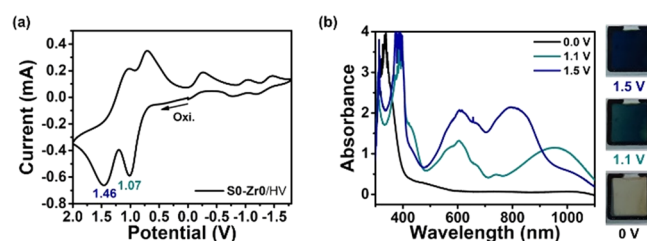


Figure 8. (a) Cyclic voltammogram and (b) spectroelectrochemical spectra of ECD based on S0-Zr0/HV (thickness: 650 \pm 15 nm, coated area: 2 cm \times 2 cm) with 0.015 M HV, 0.1 M TBABF₄, and 0.048 mL of PC at a scan rate of 50 mV/s.

TPPA moieties at the first oxidation stage to yield HV⁺, and then the resulting HV⁺ could release electrons back to the cation radical of TPPA again during the reduction process.³⁷ As a result, the existence of HV in the ECD could not only lower the oxidation potential but also enhance the switching response capability as well. Therefore, the EC behaviors of ECDs below would be carried out with HV.

The cyclic voltammetry (CV) measurements of ECDs derived from S0-Zr0/HV, S30-Zr0/HV, S0-Zr20/HV, and S30-Zr20/HV at their first redox states were investigated as shown in Figure 9, and the corresponding potential values are summarized in Table 2. According to the results, both the porous structure (S30-Zr0/HV) and hybrid system (S0-Zr20/HV) could reduce the oxidation potential from 1.07 to 1.05 and 0.99 V, respectively. Moreover, if the two approaches were combined as one system (S30-Zr20/HV), the oxidation potential could be even lowered to 0.94 V, indicating the synergistic effect of the porous hybrid film. One point is

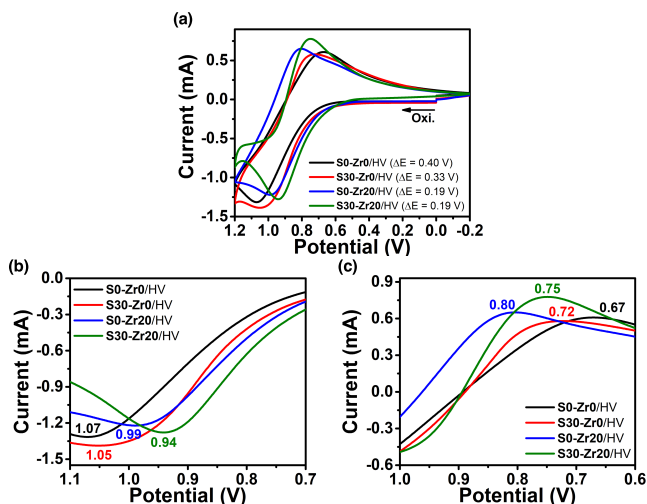


Figure 9. (a) Cyclic voltammograms, and partially magnified (b) oxidation peaks and (c) reduction peaks of ECDs S0-Zr0/HV (thickness: 650 ± 15 nm), S30-Zr0/HV (thickness: 1010 ± 20 nm), S0-Zr20/HV (thickness: 950 ± 15 nm), and S30-Zr20/HV (thickness: 1630 ± 65 nm) (active area: 2×2 cm) at a scan rate of 50 mV/s with 0.1 M TBABF₄ and 0.015 M HV in 0.048 mL of PC.

Table 2. Redox Peak Potentials of ECDs Derived from S0-Zr0/HV, S0-Zr20/HV, S30-Zr0/HV, and S30-Zr20/HV

device	$E_{\text{oxi.}}^a$ [V]	$E_{\text{red.}}^b$ [V]	ΔE^c [V]	t_c^d [s]	t_b^e [s]
S0-Zr0/HV	1.07	0.67	0.40	81.3	44.7
S30-Zr0/HV	1.05	0.72	0.33	15.9	39.8
S0-Zr20/HV	0.99	0.80	0.19	14.8	35.6
S30-Zr20/HV	0.94	0.75	0.19	9.7	20.8

^aOxidation potential at the peak. ^bReduction potential at the peak. ^cPotential difference between oxidation and reduction peaks, $|E_{\text{oxi.}} - E_{\text{red.}}|$. ^dColoring time needed from the bleaching state to 90% of total transmittance change. ^eBleaching time needed from the coloring state to 90% of total transmittance change.

worthy of noting that ΔE of the ECDs was smaller than that of the corresponding EC films due to the incorporation of HV.

2.3.2. Spectroelectrochemistry. The spectroelectrochemical spectra of S0-Zr0/HV illustrated in Figure 8b demonstrate that the optical absorption behavior of ECD was the same as the results of the corresponding polymer film measured in the liquid-type electrolyte system and also revealed the characteristic absorption peak of HV⁺ at around 606 nm. The spectra indicate that the first oxidation state is around 1.1 V, while the second one is about 1.5 V, which could correspond to the CV results in Figure 8a.

As mentioned above, the EC switching response of the obtained ECDs could be acquired by recording the difference of the optical transmittance as a function of time between the coloring and bleaching states repeatedly. Herein, to ensure a complete oxidation for EC films, 1.2 V was applied to the devices for coloring, while -0.1 V was used for bleaching to facilitate the bleaching process.

2.3.3. Electrochemical Switching Properties. A specified wavelength, 800 nm, was monitored during the redox process; the results are displayed in Figure 10. The coloring and bleaching times of S0-Zr0/HV (Figure 10a) are 81.3 and 44.7 s, respectively, while the switching times of ECDs derived from S30-Zr0/HV and S0-Zr20/HV (Figure 10b,c) both revealed faster response characteristics compared with the one from S0-

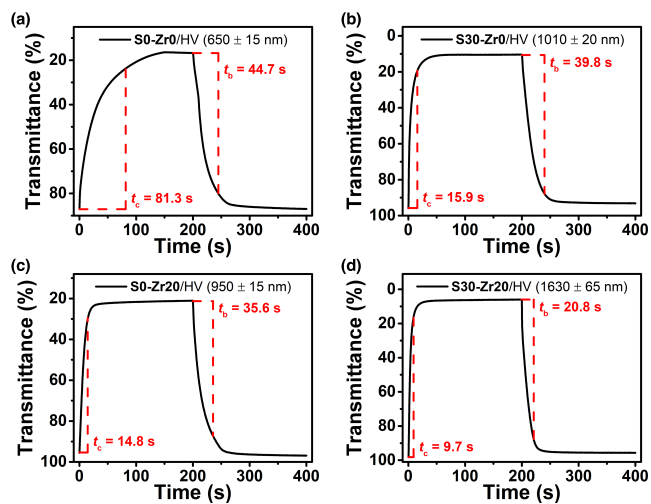


Figure 10. Switching time of ECDs (a) S0-Zr0/HV (thickness: 650 ± 15 nm), (b) S30-Zr0/HV (thickness: 1010 ± 20 nm), (c) S0-Zr20/HV (thickness: 950 ± 15 nm), and (d) S30-Zr20/HV (thickness: 1630 ± 65 nm) (active area: 2×2 cm) at 800 nm with the coloring voltage of 1.2 V and bleaching voltage of -0.1 V with 0.1 M TBABF₄ and 0.015 M HV in 0.048 mL of PC.

Zr0/HV. Additionally, S30-Zr20/HV exhibited an even shorter coloring time of 9.7 s and bleaching time of 20.8 s (Figure 10d) than the two modified devices of S30-Zr0/HV and S0-Zr20/HV, confirming the promising combination effect of the porous structure and hybrid system.

The switching stability of S30-Zr20/HV was also investigated at a cycle time of 200 s (including coloring time and bleaching time) for 100 cycles. The applied coloring voltages were 1.2 and -0.1 V for the bleaching voltage. The result is shown in Figure 11. The decay of transmittance change was only less than 1% after 100 cycles, manifesting the promising electrochemical stability of the ECD based on S30-Zr20/HV.

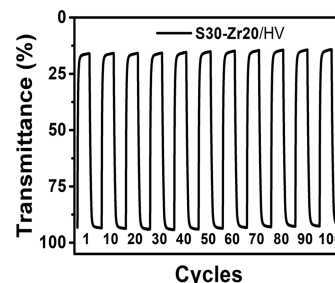


Figure 11. Switching capability of ECD based on S30-Zr20/HV (thickness: 1630 ± 65 nm) between 1.2 and -0.1 V at 800 nm with a cycle of 200 s for 100 cycles with 0.1 M TBABF₄ and 0.015 M HV in 0.048 mL of PC.

3. CONCLUSIONS

Three types of polymer films, including the porous structure, hybrid system, and porous hybrid combination films, were all successfully prepared and compared in this study. Both the porous films and hybrid films showed the same tendency as the previous study: both coloring time and bleaching time were shortened, and the oxidation potential could also be lowered effectively. Furthermore, from the results of redox potentials and switching response time, the approach of hybrid system

revealed to be more effective for the enhancement of EC response behaviors than the method of salt-forming porous structure that might be attributed to the faster electron transfer via the assistance of ZrO_2 linked to the polymer backbone through covalent bonds during the redox process. It is noteworthy that the porous hybrid film **S30-Zr20** combining two modifications exhibited the synergistic effect of the porous structure and hybrid system, demonstrating the lowest oxidation potential (0.37 V) and the shortest switching response times (coloring time of 6.4 s and bleaching time of 14.9 s). Furthermore, EIS was also measured and the values of charge transfer resistance (R_{ct}) were compared to give a more convincing evidence for the enhancement of switching capability of these modified EC films, and the obtained EIS measurements could be related to the switching response behaviors. For further applications, some representative EC films were chosen to fabricate the ECDs. With the help of HV and the porous hybrid structure, the enhancement of EC behaviors obtained in ECDs exhibited the similar trend to the corresponding one-layer EC films. Consequently, the EC materials with enhanced response capability and operating stability could be obtained by integrating the porous structure and metal oxide hybrid, which would have the synergistic effect and result in better improvement in EC behaviors than either the porous structure or organic–inorganic hybrid system.

4. EXPERIMENTAL SECTION

4.1. Materials. *N,N'*-Bis(4-aminophenyl)-*N,N'*-di-(methoxyphenyl)-1,4-phenylenediamine (**TPPA**) was prepared according to a previous study.³⁸ The supporting electrolyte of TBABF_4 for electrochemical measurement was prepared as follows: the tetrabutylammonium bromide (TBABr) aqueous solution was added to the saturated sodium tetrafluoroborate (NaBF_4) aqueous solution drop by drop under vigorous stirring. Then, the white precipitate was collected and purified with 1:2 ethanol/water mixture. The cathodic EC material HV was also prepared as follows: heptyl viologen dibromide (HVBr_2) was first prepared by adding 4,4'-dipyridyl and 1-bromoheptane to acetonitrile and refluxing the mixture for several hours, and the yellow precipitate was filtered and washed with chloroform. Then, it was dissolved in DI water and dropped into the saturated aqueous solution of NaBF_4 , and the resulting white precipitate was collected and recrystallized with ethanol. Commercially available *N,N*-dimethylacetamide (DMAc) (TEDIA), triphenyl phosphite (TPP) (ACROS), pyridine (Py) (ACROS), and other reagents were used as received.

4.2. Synthesis of TPPA-A. Adipic acid (0.29 g, 2 mmol) was first added to 5.1 mL of NMP (20 wt %). Then, 0.4 mL of pyridine, 0.5 g of CaCl_2 , 1.4 mL of TPP, and 1.01 g of **TPPA** (2 mmol) were added to the solution. The mixture was stirred at 105 °C for 4 h. After cooling down to room temperature, the whole solution was poured into 3:1 methanol/water mixture to obtain the fiber-like precipitation of the polymer. The precipitation was filtered and purified by Soxhlet extraction with methanol for 1 day and dried at 100 °C under vacuum.

4.3. Synthesis of TPPA-M.²⁹ During the polycondensation, the hydroxyl groups of malic acid may react with the carboxylic groups of the diacid at 105 °C and cause a side reaction. Therefore, the reaction temperature was lowered to 60 °C with a longer reaction time. Besides the reaction temperature and time, the synthesis procedure is the same as **TPPA-A**. Malic acid (0.27 g, 2 mmol), 0.4 mL of pyridine, 0.5 g of CaCl_2 , 1.4 mL of TPP, and 1.01 g of **TPPA** (2 mmol) were added to 5.0 mL of NMP (20 wt %). The mixture was stirred at 60 °C for 12 h. Then, the polymer was precipitated with 3:1 methanol/water mixture and filtered. The obtained fiber-like precipitation was purified by Soxhlet extraction with methanol for 24 h and dried in vacuum at 100 °C.

4.4. Fabrication of the Electrochromic Films and Devices.

The preparation of different kinds of films is shown in Figure S1, and the fabrication of ECDs is as follows. The EC polyamide film was first coated on a 2.5×3 cm ITO glass as an anode. Then, another piece of ITO glass with the same size was taken as a cathode, and a 2×2 cm thermosetting plastic frame with a 1 cm width break is dispensed by a full-auto dispenser. The two glasses are glued together to form an ECD with a gap of around 120 μm and the device is baked under 125 °C for 6 h. Next, the polymer conductive gel is injected into the device from the 1 cm width break through the vacuum encapsulation method and the break is sealed with UV gel. The polymer gel is prepared with 275 mg of poly(methyl methacrylate) (PMMA, M_w : 120,000), 66 mg of TBABF_4 (0.1 M), 15.8 mg of HV (0.015 M), and 2 mL of propylene carbonate (PC). The total volume of the gel injected is about 0.048 mL.

4.5. Measurements. Inherent viscosities of the polymers with a concentration of 0.5 g/dL DMAc were measured by glass capillary viscometers in a Tamson TV2000 viscometer bath at 30 °C. Molecular weights are measured by gel permeation chromatographic (GPC) analysis carried out on a Waters chromatography unit interfaced with a Waters 2410 refractive index detector. Two Shodex GPC KD-803 and GPC KD-804 were connected in series with NMP and LiCl salt (20 mM) as the eluent at a flow rate of 0.35 mL/min at 40 °C and calibrated with polystyrene standards. Transparency of the polymer films was measured using a Jasco V-650 UV–vis spectrophotometer. The surface structure of porous films was observed using a JOEL JSM-6700F field emission scanning electron microscope. Electrochemical measurements, including cyclic voltammetry (CV) and electrochemical impedance spectroscopy (EIS), were conducted using a CH Instruments 6122E Electrochemical Analyzer under a three-electrode system consisting of a polymer film coated on a 0.6×3 cm ITO glass as a working electrode, a platinum counter electrode, and a Ag/Ag^+ reference electrode in 3 mL of anhydrous acetonitrile with 0.1 M TBABF_4 as a supporting electrolyte. The scanning rate of CV was 50 mV/s, and EIS was tested in the frequency from 1 MHz to 1 Hz. The absorption spectra of spectroelectrochemical measurements were recorded using an Agilent UV–vis spectrophotometer.

■ ASSOCIATED CONTENT

Supporting Information

The Supporting Information is available free of charge at <https://pubs.acs.org/doi/10.1021/acsami.0c09314>.

Preparation routes of porous films, hybrid films, and porous hybrid films; UV–vis spectra of porous films of **TPPA-A** and **TPPA-M**; spectroelectrochemical spectra of **S0-Zr0**; CV diagrams and switching response time at 920 nm of the resulting films (PDF)

■ AUTHOR INFORMATION

Corresponding Author

Guey-Sheng Liou – Institute of Polymer Science and Engineering and Advanced Research Center for Green Materials Science and Technology, National Taiwan University, Taipei 10617, Taiwan; orcid.org/0000-0003-3725-3768; Phone: +886-2-33665070; Email: gsliou@ntu.edu.tw

Authors

Ya-Wen Chiu – Institute of Polymer Science and Engineering and Advanced Research Center for Green Materials Science and Technology, National Taiwan University, Taipei 10617, Taiwan

Min-Hao Pai – Institute of Polymer Science and Engineering, National Taiwan University, Taipei 10617, Taiwan

Complete contact information is available at: <https://pubs.acs.org/doi/10.1021/acsami.0c09314>

Notes

The authors declare no competing financial interest.

ACKNOWLEDGMENTS

Y.-W.C. and G.-S.L. received financial support from “Advanced Research Center for Green Materials Science and Technology” from the Featured Area Research Center Program within the framework of the Higher Education Sprout Project by the Ministry of Education (109L9006) and the Ministry of Science and Technology in Taiwan (MOST 109-2634-F-002-042). Y.-W.C., M.-H.P., and G.-S.L. received financial support from the Ministry of Science and Technology in Taiwan (MOST 107-2113-M-002-024-MY3 and 107-2221-E-002-066-MY3).

REFERENCES

- (1) Deb, S. K. A Novel Electrophotographic System. *Appl. Opt.* **1969**, *8*, 192–195.
- (2) Platt, J. R. Electrochromism, a possible change of color producible in dyes by an electric field. *J. Chem. Phys.* **1961**, *34*, 862–863.
- (3) Weil, M.; Schubert, W.-D. The beautiful colours of tungsten oxides. *Int. Tungsten Ind. Assoc.* **2013**, 1–9.
- (4) Carpenter, M. K.; Conell, R. S.; Corrigan, D. A. The electrochromic properties of hydrous nickel oxide. *Sol. Energ. Mater.* **1987**, *16*, 333–346.
- (5) Estrada, W.; Andersson, A. M.; Granqvist, C. G. Electrochromic nickel-oxide-based coatings made by reactive dc magnetron sputtering: Preparation and optical properties. *J. Appl. Phys.* **1988**, *64*, 3678–3683.
- (6) Svensson, J. S. E. M.; Granqvist, C. G. Optical properties of electrochromic hydrated nickel oxide coatings made by rf sputtering. *Appl. Opt.* **1987**, *26*, 1554–1556.
- (7) Mortimer, R. J.; Rosseinsky, D. R. Iron hexacyanoferrate films: spectroelectrochemical distinction and electrodeposition sequence of ‘soluble’ (K⁺-containing) and ‘insoluble’ (K⁺-free) Prussian Blue, and composition changes in polyelectrochromic switching. *J. Chem. Soc., Dalton Trans.* **1984**, *9*, 2059–2062.
- (8) Neff, V. D. Electrochemical oxidation and reduction of thin films of Prussian Blue. *J. Electrochem. Soc.* **1978**, *125*, 886.
- (9) Michaelis, L.; Hill, E. S. The viologen indicators. *J. Gen. Physiol.* **1933**, *16*, 859–873.
- (10) Stargardt, J. F.; Hawkridge, F. M. Computer decomposition of the ultraviolet-visible absorption spectrum of the methyl viologen cation radical and its dimer in solution. *Anal. Chim. Acta* **1983**, *146*, 1–8.
- (11) Rourke, F.; Crayston, J. A. Cyclic voltammetry and morphology of polyaniline-coated electrodes containing [Fe(CN)₆]^{3−/4−} ions. *J. Chem. Soc., Faraday Trans.* **1993**, *89*, 295–302.
- (12) Sherman, B. C.; Euler, W. B.; Force, R. R. The modern student laboratory: polyaniline-A conducting polymer: electrochemical synthesis and electrochromic properties. *J. Chem. Educ.* **1994**, *71*, A94–A96.
- (13) Han, F. S.; Higuchi, M.; Kurth, D. G. Metallo-Supramolecular Polymers Based on Functionalized Bis-terpyridines as Novel Electrochromic Materials. *Adv. Mater.* **2007**, *19*, 3928–3931.
- (14) Leasure, R. M.; Ou, W.; Moss, J. A.; Linton, R. W.; Meyer, T. J. Spatial electrochromism in metallopolymeric films of ruthenium polypyridyl complexes. *Chem. Mater.* **1996**, *8*, 264–273.
- (15) Yen, H. J.; Liou, G. S. Recent advances in triphenylamine-based electrochromic derivatives and polymers. *Polym. Chem.* **2018**, *9*, 3001–3018.
- (16) Chiu, K. Y.; Su, T. X.; Li, J. H.; Lin, T.-H.; Liou, G.-S.; Cheng, S.-H. Novel trends of electrochemical oxidation of amino-substituted triphenylamine derivatives. *J. Electroanal. Chem.* **2005**, *575*, 95–101.
- (17) Liu, H. S.; Pan, B. C.; Huang, D. C.; Kung, Y. R.; Leu, C. M.; Liou, G. S. Highly transparent to truly black electrochromic devices based on an ambipolar system of polyamides and viologen. *NPG Asia Mater.* **2017**, *9*, No. e388.
- (18) Wu, J. T.; Liou, G. S. A novel panchromatic shutter based on an ambipolar electrochromic system without supporting electrolyte. *Chem. Commun.* **2018**, *54*, 2619–2622.
- (19) Lu, C.-H.; Hon, M. H.; Leu, I.-C. Direct Growth of Crystalline Tungsten Oxide Nanorod Arrays by a Hydrothermal Process and Their Electrochromic Properties. *J. Electron. Mater.* **2017**, *46*, 2080–2084.
- (20) Cai, G.; Cui, M.; Kumar, V.; Darmawan, P.; Wang, J.; Wang, X.; Eh, A. L.-S.; Qian, K.; Lee, P. S. Ultra-large optical modulation of electrochromic porous WO₃ film and the local monitoring of redox activity. *Chem. Sci.* **2016**, *7*, 1373–1382.
- (21) Zhou, S.; Wang, S.; Zhou, S.; Xu, H.; Zhao, J.; Wang, J.; Li, Y. An electrochromic supercapacitor based on an MOF derived hierarchical-porous NiO film. *Nanoscale* **2020**, *12*, 8934–8941.
- (22) Liang, H.; Li, R.; Li, C.; Hou, C.; Li, Y.; Zhang, Q.; Wang, H. Regulation of carbon content in MOF-derived hierarchical-porous NiO@C films for high-performance electrochromism. *Mater. Horiz.* **2019**, *6*, 571–579.
- (23) Roy, S.; Chakraborty, C. Nanostructured metallo-supramolecular polymer-based gel-type electrochromic devices with ultrafast switching time and high colouration efficiency. *J. Mater. Chem. C* **2019**, *7*, 2871–2879.
- (24) Xiong, S.; Phua, S. L.; Dunn, B. S.; Ma, J.; Lu, X. Covalently bonded polyaniline-TiO₂ hybrids: a facile approach to highly stable anodic electrochromic materials with low oxidation potentials. *Chem. Mater.* **2010**, *22*, 255–260.
- (25) Huang, B. R.; Lin, T. C.; Liu, Y. M. WO₃/TiO₂ core-shell nanostructure for high performance energy-saving smart windows. *Sol. Energy Mater. Sol. Cells* **2015**, *133*, 32–38.
- (26) Roy, S.; Chakraborty, C. Sub-second electrochromic switching and ultra-high coloration efficiency in halloysite nanoclay incorporated metallo-supramolecular polymer nano-hybrid based electrochromic device. *Sol. Energy Mater. Sol. Cells* **2020**, *208*, 110392.
- (27) Xu, H.; Gong, L.; Zhou, S.; Cao, K.; Wang, S.; Zhao, J.; Li, Y. Enhancing the electrochromic stability of Prussian blue based on TiO₂ nanorod arrays. *New J. Chem.* **2020**, *44*, 2236–2240.
- (28) Pan, B. C.; Chen, W. H.; Hsiao, S. H.; Liou, G. S. A facile approach to prepare porous polyamide films with enhanced electrochromic performance. *Nanoscale* **2018**, *10*, 16613–16620.
- (29) Pan, B. C.; Chen, W. H.; Lee, T. M.; Liou, G. S. Synthesis and characterization of novel electrochromic devices derived from redox-active polyamide–TiO₂ hybrids. *J. Mater. Chem. C* **2018**, *6*, 12422–12428.
- (30) Lee, S. H.; Deshpande, R.; Parilla, P. A.; Jones, K. M.; To, B.; Mahan, A. H.; Dillon, A. C. Crystalline WO₃ Nanoparticles for Highly Improved Electrochromic Applications. *Adv. Mater.* **2006**, *18*, 763–766.
- (31) Wang, J.; Khoo, E.; Lee, P. S.; Ma, J. Synthesis, Assembly, and Electrochromic Properties of Uniform Crystalline WO₃ Nanorods. *J. Phys. Chem. C* **2008**, *112*, 14306–14312.
- (32) Xiong, C.; Aliev, A. E.; Gnade, B.; Balkus, K. J., Jr. Fabrication of Silver Vanadium Oxide and V₂O₅ Nanowires for Electrochromics. *ACS Nano* **2008**, *2*, 293–301.
- (33) Liou, G. S.; Lin, P. H.; Yen, H. J.; Yu, Y. Y.; Chen, W. C. Flexible nanocrystalline-titania/polyimide hybrids with high refractive index and excellent thermal dimensional stability. *J. Polym. Sci.* **2010**, *48*, 1433–1440.
- (34) Liou, G. S.; Lin, P. H.; Yen, H. J.; Yu, Y. Y.; Tsai, T. W.; Chen, W. C. Highly flexible and optical transparent 6F-PI/TiO₂ optical hybrid films with tunable refractive index and excellent thermal stability. *J. Mater. Chem.* **2010**, *20*, 531–536.
- (35) Nicholson, R. S.; Shain, I. Theory of stationary electrode polarography. Single scan and cyclic methods applied to reversible, irreversible, and kinetic systems. *Anal. Chem.* **1964**, *36*, 706–723.
- (36) Orazem, M. E.; Tribollet, B. *Electrochemical Impedance Spectroscopy*, John Wiley & Sons, 2017.

- (37) Wu, J. H.; Liou, G. S. High-Performance Electrofluorochromic Devices Based on Electrochromism and Photoluminescence-Active Novel Poly (4-Cyanotriphenylamine). *Adv. Funct. Mater.* **2014**, *24*, 6422–6429.
- (38) Yen, H. J.; Liou, G. S. *Chem. of Mater.* **2009**, *21*, 4062–4070.